UCLA/13/TEP/101 SB/F/420-13 SLAC-PUB-15395

IPPP-13-16 FR-PHENO-2013-004

Next-to-Leading Order $W + 5$-Jet Production at the LHC

Z. Bern[a], L. J. Dixon[b], F. Febres Cordero[c], S. Höche[b],

H. Ita[d], D. A. Kosower[e], D. Maître[f] and K. J. Ozeren[a]

[a]Department of Physics and Astronomy, UCLA, Los Angeles, CA 90095-1547, USA

[b]SLAC National Accelerator Laboratory, Stanford University, Stanford, CA 94309, USA

[c]Departamento de Física, Universidad Simón Bolívar, Caracas 1080A, Venezuela

[d]Physikalisches Institut, Albert-Ludwigs-Universität Freiburg, D–79104 Freiburg, Germany

[e]Institut de Physique Théorique, CEA–Saclay, F–91191 Gif-sur-Yvette cedex, France

[f]Department of Physics, University of Durham, Durham DH1 3LE, UK

Abstract

We present next-to-leading order QCD predictions for the total cross section and for a comprehensive set of transverse-momentum distributions in $W + 5$-jet production at the Large Hadron Collider. We also present ratios of total cross sections, and use them to obtain an extrapolation formula to an even larger number of jets. We include the decay of the W boson into leptons. This is the first such computation with six final-state vector bosons or jets. We use BlackHat together with SHERPA to carry out the computation.

PACS numbers: 12.38.-t, 12.38.Bx, 13.87.-a, 14.70.Fm

Work supported by US Department of Energy contract DE-AC02-76SF00515 and HEP.

I. INTRODUCTION

Reliable theoretical predictions for Standard-Model processes at the Large Hadron Collider (LHC) are important to ongoing searches for new physics. They are also important to the increasingly precise studies of the newly discovered Higgs-like boson [1, 2], of the top quark, and of vector boson self-interactions. New-physics signals very typically lie beneath Standard-Model backgrounds in a broad range of search strategies. Ferreting out the signals requires a good quantitative understanding of the backgrounds and their uncertainties. With the increasing jet multiplicities used in cutting-edge search strategies, this becomes more and more challenging. Some of the uncertainty surrounding predictions of Standard-Model background rates can be alleviated through use of data-driven estimates, but this technique also requires theoretical input to predict the ratios of background processes in signal regions to those for control processes or in control regions.

Predictions for background rates at the LHC rely on perturbative QCD, which enters all aspects of short-distance collisions at a hadron collider. Leading-order (LO) predictions in QCD suffer from a strong dependence on the unphysical renormalization and factorization scales. This dependence gets stronger with increasing jet multiplicity. Next-to-leading (NLO) results generally reduce this dependence dramatically, typically to a 10-15% residual sensitivity. Thus they offer the first quantitatively reliable order in perturbation theory.

The production of a W boson in association with jets has played a special role in collider physics. It was the dominant background to top-quark pair production at the Tevatron. At the LHC it remains an important background for precision studies, including those of top quarks. It is important to many new physics searches involving missing energy, including those for supersymmetry. Recent searches have made use of samples with high jet multiplicity, and proposed searches aim to push to higher multiplicities yet. Precise quantitative control over the theoretical predictions leads to improved sensitivity to new phenomena. Measurements of W boson production in association with multiple jets have been made by the CDF [3] and D0 [4] collaborations at the Tevatron, and by the ATLAS [5, 6] and CMS [7] collaborations at the LHC. Such measurements also permit stringent tests of the predictions of the Standard Model.

Theoretical predictions for the production of vector bosons with a lower multiplicity of jets (one or two jets) have been available at NLO in QCD for many years [8–10]. In recent

years, the advent of new on-shell techniques [11–19] for computing one-loop amplitudes at larger multiplicity has led to NLO results for three [20–23] and four [24, 25] associated jets. Other new results include those for the production of vector-boson pairs [26] or top–anti-top pairs [27, 28] in association with two jets. Another recent approach [29] has been demonstrated in the production of up to seven jets in e^+e^- collisions, and shows promise for LHC physics as well. There have also been important advances with more traditional methods, especially for the case of heavy quarks [27, 30, 31]. In the present article, we take another step forward in multiplicity, presenting NLO results for inclusive W + 5-jet production at the LHC. These are the first NLO QCD results at a hadron collider with six or more electroweak bosons or jets in the final state. We incorporate the decay of the W boson into leptons, so that there are seven final-state objects to track.

In the present paper we use on-shell methods as implemented in numerical form in the BlackHat software library [32]. This library, together with the SHERPA package [33], has previously been used to make NLO predictions for $W, Z/\gamma^*$ + 3-jet production [22, 23], for $W, Z/\gamma^*$ + 4-jet production [24, 25], and for four-jet production [34]. It has also been used in investigations of high-$p_{\rm T}$ W polarization [35], and to compute γ + n-jet to Z + n-jet ratios for assessing theoretical uncertainties [36, 37] in the CMS searches [38] for supersymmetric particles. The ATLAS collaboration has also used results from BlackHat computations with SHERPA for Standard-Model studies of electroweak vector-boson production in association with three or more jets [6]. Other programs that use on-shell methods are described in refs. [39].

SHERPA is used to manage the numerous partonic subprocesses entering the calculation, to integrate over phase space, to construct physical distributions, and to output root [40] n-tuples. In contrast to earlier computations, we use the COMIX package [41] to compute Born and real-emission matrix elements, along with the Catani–Seymour [42] dipole subtraction terms. Rather than repeating the entire computation for each scale and for each parton distribution function (PDF) set, we store intermediate results in n-tuple format, recording momenta for all partons in an event, along with the coefficients of various scale- or PDF-dependent functions in the event weight. The n-tuple storage makes it possible to evaluate cross sections and distributions for different scales and PDF error sets. We perform the basic calculation with loose cuts, also making it possible to choose different (tighter) cuts without recomputing the time-consuming matrix elements.

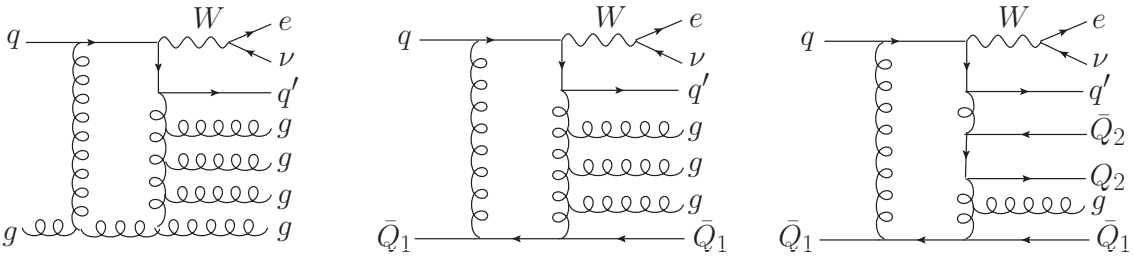

FIG. 1: Sample eight-point loop diagrams for the processes $qg \to Wq'gggg$, $q\bar{Q}_1 \to Wq'ggg\bar{Q}_1$ and $q\bar{Q}_1 \to Wq'\bar{Q}_2Q_2g\bar{Q}_1$, followed by the decay of the W boson to leptons.

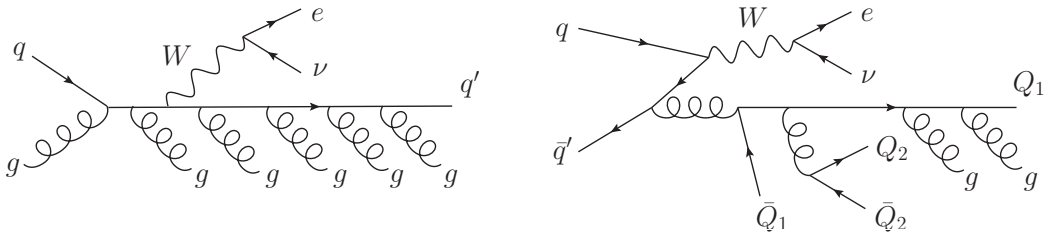

FIG. 2: Sample nine-point real-emission diagrams for the processes $qg \to Wq'ggggg$ and $q\bar{q}' \to W\,Q_1ggQ_2\bar{Q}_2\bar{Q}_1$, followed by the decay of the W boson to leptons.

In this paper, we compute the total cross sections at NLO for inclusive $W^+ + n$-jet and $W^- + n$-jet production with $n \leq 5$ and describe W^+/W^- ratios and $W + n$-jet/$W+$ $(n-1)$-jet ratios. Such ratios can be sensitive probes of new physics. We also study two types of distributions: the differential cross section in the total hadronic transverse energy $H_{\mathrm{T}}^{\mathrm{jets}} = \sum_{j\in\mathrm{jets}} p_{\mathrm{T}}^j$, and the complete set of differential cross sections in the jet transverse momenta. For four and five jets we make use of a leading-color approximation for the virtual contributions. This approximation has been shown to have subleading-color corrections of under 3% for processes with four or fewer associated jets [22, 43].

This paper is organized as follows. In section II we summarize the basic setup of the computation. In section III we present our results for cross sections, ratios and distributions. We give our summary and conclusions in section IV.

II. BASIC SETUP

In this paper we compute the W + 5-jet processes in NLO QCD, followed by leptonic W-boson decay,

$$\begin{aligned} pp &\longrightarrow W^- + 5 \text{ jets} \to e^- \bar{\nu}_e + 5 \text{ jets}\,, \\ pp &\longrightarrow W^+ + 5 \text{ jets} \to e^+ \nu_e + 5 \text{ jets}\,. \end{aligned} \tag{2.1}$$

These processes receive contributions from several partonic subprocesses. At leading order, and in the virtual NLO contributions, the W^- subprocesses are all obtained from

$$\begin{aligned} &q\bar{q}'gggg \to W^- \to e^-\,\bar{\nu}_e\,, \\ &q\bar{q}'Q_1\bar{Q}_1gg \to W^- \to e^-\,\bar{\nu}_e\,, \\ &q\bar{q}'Q_1\bar{Q}_1Q_2\bar{Q}_2g \to W^- \to e^-\,\bar{\nu}_e\,, \end{aligned} \tag{2.2}$$

by crossing five of the partons into the final state. Similarly, we obtain the subprocesses for the W^+ case from the various crossings of the subprocesses

$$\begin{aligned} &q\bar{q}'gggg \to W^+ \to e^+\,\nu_e\,, \\ &q\bar{q}'Q_1\bar{Q}_1gg \to W^+ \to e^+\,\nu_e\,, \\ &q\bar{q}'Q_1\bar{Q}_1Q_2\bar{Q}_2g \to W^+ \to e^+\,\nu_e\,. \end{aligned} \tag{2.3}$$

The W boson changes the quark flavor and couples to the q-q' line. Both the labels q and Q_i denote light quarks. Amplitudes with multiple identical quark flavors are obtained by appropriate symmetrization. Sample Feynman diagrams illustrating virtual contributions with 1, 2 and 3 external quark pairs are shown in fig. 1 (although our calculation is not based on Feynman diagrams). All contributions to the virtual corrections are included in a leading-color approximation described below. Besides the virtual contributions, NLO QCD requires also real-emission contributions with an additional parton in the final state. Here we keep the full color dependence. However, we drop the finite contributions from tree amplitudes with four external quark pairs; they contribute well under 1% to the cross section. Sample real-emission diagrams are displayed in fig. 2.

The decay of the vector boson ($W^\pm$) into a charged lepton and neutrino is included at the amplitude level; no on-shell approximation is made for the W boson. The lepton-pair invariant mass follows a relativistic Breit-Wigner distribution with width given by

$\Gamma_W = 2.06$ GeV and mass $M_W = 80.419$ GeV. (The other electroweak parameters are also chosen as in ref. [22].) We take the leptonic decay products to be massless. In this approximation, of course, the results for muon final states are identical to those for electrons. The five light quarks, u, d, c, s, b, are all treated as massless. We do not include contributions to the amplitudes from a real or virtual top quark; its omission should have a percent-level effect on the overall result [24, 25]. We also approximate the Cabibbo-Kobayashi-Maskawa matrix by the unit matrix. As previously determined for the three-jet case, this approximation causes a change of under 1% in total cross sections for the cuts we impose [22], and should also be completely negligible in our study.

A. Kinematics and Observables

We use standard kinematic variables, whose definitions may be found in Appendix A of ref. [23]. The renormalization and factorization scales in ref. [22] were chosen as multiples of a total partonic transverse energy $\hat{H}_{\rm T}$. We will use a modified version of it here,

$$\hat{H}'_{\rm T} \equiv \sum_m p_{\rm T}^m + E_{\rm T}^W \,, \tag{2.4}$$

where the sum runs over all final-state partons m and $E_{\rm T}^W \equiv \sqrt{M_W^2 + (p_{\rm T}^W)^2}$. All partons m are included in $\hat{H}'_{\rm T}$, whether or not they are inside jets that pass the cuts. This quantity is not directly measurable; however, it is very similar to the more usual jet-based total transverse energy, and it is more practical for use as a dynamical scale choice. Both $\hat{H}_{\rm T}$ and the modified version $\hat{H}'_{\rm T}$ are independent of the experimental cuts. Thus, modifying the cuts will not affect the value of the matrix element at a point in phase space. This makes it suitable as a choice of renormalization or factorization scale, avoiding unwanted dependence on experimental cuts. Later we will compute the distribution in the jet-based observable $H_{\rm T}^{\rm jets} = \sum_{j \in {\rm jets}} p_{\rm T}^j$. This variable is similar to the partonic version, $\hat{H}'_{\rm T}$, except that the W boson $E_{\rm T}$ is omitted, and it is based on jets passing all cuts.

We define jets using the anti-k_T algorithm [44] with parameter $R = 0.5$. The jets are ordered in $p_{\rm T}$, and are labeled $i, j = 1, 2, 3, \ldots$ in order of decreasing transverse momentum $p_{\rm T}$, with jet 1 being the leading (hardest) jet. The transverse mass of the W boson is computed from the transverse momenta of its leptonic decay products, $M_{\rm T}^W = \sqrt{2E_{\rm T}^e E_{\rm T}^\nu (1 - \cos(\Delta\phi_{e\nu}))}$.

In our study, we consider the inclusive process $pp \to W + 5$ jets at an LHC center-of-mass energy of $\sqrt{s} = 7$ TeV with the following set of cuts:

$$\begin{aligned} &E_{\rm T}^e > 20 \text{ GeV}\,, \qquad &&|\eta^e| < 2.5\,, \qquad &&\not{E}_{\rm T} > 20 \text{ GeV}\,, \\ &p_{\rm T}^{\rm jet} > 25 \text{ GeV}\,, \qquad &&|\eta^{\rm jet}| < 3\,, \qquad &&M_{\rm T}^W > 20 \text{ GeV}\,. \end{aligned} \tag{2.5}$$

In this study we take the missing transverse energy, $\not{E}_{\rm T}$, to equal the neutrino transverse energy, $E_{\rm T}^\nu$.

In carrying out the computation we imposed a set of looser cuts and generated ROOT [40] format n-tuples. As mentioned above and described further below, the n-tuples store intermediate results such as parton momenta and coefficients associated with the event weights for the events passing the looser cuts, whose only restriction is that the minimum jet transverse momentum is $p_{\rm T}^{\rm jet} > 25$ GeV. The n-tuples are also valid for anti-k_T, k_T and SISCone algorithms [44, 45] for $R = 0.4, 0.5, 0.6, 0.7$, as implemented in the FASTJET package [46]. In the SISCone case the merging parameter f is chosen to be 0.75. This allows the n-tuples to be used for studying the effects of varying the jet algorithm, along with variations due to parton distributions, scale choices, and experimental cuts.

In our study, we use the MSTW2008 LO and NLO PDFs [47] at the respective orders. We use the five-flavor running $\alpha_s(\mu)$ and the value of $\alpha_s(M_Z)$ supplied with the parton distribution functions.

Our predictions are at parton level. We do not apply corrections due to non-perturbative effects such as those induced by the underlying event or hadronization. For comparisons to experiment it is important to incorporate these effects, although for most cross-section ratios we do not expect them to be large. Parton-shower event generators such as POWHEG and MC@NLO [48], and further refinements of these methods [49], have been developed that consistently include a parton shower and maintain NLO accuracy for events with a specified jet multiplicity. More recently, advances have been made in maintaining the NLO accuracy across different jet multiplicities in a single sample [50]. These advances mark an important step in significantly reducing theoretical uncertainties associated with hadron-level predictions of many types of LHC events. We look forward to applying them in the future to the production of W bosons with up to five additional jets.

B. Formalism and Software

The new techniques we use for obtaining virtual contributions are collectively known as on-shell methods, and are reviewed in refs. [51]. These methods rely on underlying properties of amplitudes — factorization and unitarity — in order to express them in terms of simpler, on-shell amplitudes of lower multiplicity. While amplitudes necessarily contain off-shell states inside loops or trees, avoiding direct use of these states allows the method to avoid the gauge dependence they induce. Eliminating the gauge dependence greatly reduces the enormous cancellations of intermediate terms that would plague a textbook Feynman-diagram calculation. The first application of the unitarity method [11] to collider physics was to obtain the analytic matrix elements for $q\bar{q}gg \to V$ and $q\bar{q}Q_1\bar{Q}_1 \to V$ ($V = W$ or Z) [13], used in the NLO program MCFM [9]. More recently, on-shell methods been implemented in a more flexible numerical form, breaking the long-standing bottleneck to NLO computations for higher-multiplicity final states posed by the one-loop (virtual) corrections. These methods scale well as the number of external legs increases [16, 20–22, 24–26, 28, 39, 52]. There have also been important advances in computing virtual corrections with more traditional methods [30].

One-loop amplitudes in QCD with massless quarks may be expressed as a sum over three different types of Feynman integrals (boxes, triangles, and bubbles) with additional so-called rational terms. The integrals are universal and well-tabulated, so the aim of the calculation is to compute their coefficients, along with the rational terms. In an on-shell approach, the integral coefficients may be computed using four-dimensional generalized unitarity [11, 13, 14], while the rational terms may be computed either by a loop-level version [16] of on-shell recursion [15] or using D-dimensional unitarity [12]. We use a numerical version [32] of Forde's method [18] for the integral coefficients, and subtract box and triangle integrands similar to the Ossola–Papadopoulos–Pittau procedure [17], improving the numerical stability. To compute the rational terms, we use a numerical implementation of Badger's massive continuation method [19], which is related to D-dimensional unitarity.

These algorithms are implemented in an enhanced version of the BlackHat code [20, 32]. BlackHat organizes the computation of the amplitudes in terms of elementary gauge-invariant "primitive amplitude" building blocks [13, 53]. Many primitive amplitudes can be associated with Feynman diagrams in which all external partons touch the loop (i.e. there

are no nontrivial trees attached to the loop). Representative Feynman diagrams for the leading-color primitive amplitudes used in the present calculation are shown in fig. 1. The primitive amplitudes are then assembled into partial amplitudes, which are the kinematic coefficients of the different color tensors that can appear in the amplitude. The complete virtual cross section is obtained by interfering the one-loop partial amplitudes with the tree-level amplitude and summing over spins and color indices. The color factors arising from the color sum in the assembly of primitive amplitudes into partial amplitudes become highly nontrivial as the number of quark lines increases; we use a general solution given in ref. [43]. An important feature is that each primitive building block has a relatively simple analytic structure with only a limited number of spurious singularities present. A given primitive amplitude can appear in multiple partial amplitudes and does not have to be recomputed for each one. This approach also allows for a straightforward separation of leading- and subleading-color contributions. This separation can be exploited to significantly enhance the efficiency of the Monte Carlo integration [22]: The subleading-color contributions are much smaller, yet more computationally costly; separating them out allows them to be evaluated at far fewer phase-space points than the leading-color contributions, in order to obtain similar absolute uncertainties.

In the $W + 4,5$-jet calculations we drop altogether the small but time-consuming subleading-color contributions to the virtual corrections. As explicitly verified for three- [22] and four-jet production [43], the omitted subleading-color contributions to the virtual corrections are typically 10% of the leading-color virtual terms, and under 3% of the total cross section. We expect the dropped subleading-color contributions to be similarly small for $W + 5$-jet production. The precise version of the leading-color approximation for the virtual terms used here is the one of ref. [43]. It retains full-color dependence in all contributions multiplying poles in the dimensional regularization parameter ϵ in the virtual corrections. In the finite parts of the virtual corrections, it drops certain contributions that are subleading in the number of colors N_c in the formal limit $N_c \to \infty$, with n_f/N_c held fixed. In particular, we drop those finite parts of the leading-color partial amplitudes that are suppressed by explicit powers of $1/N_c$, as well as all finite parts of the subleading-color partial amplitudes. In forming the color-summed interference of the surviving parts of the one-loop amplitudes with the tree amplitudes, we do not drop any further terms. The BlackHat code uses the four-dimensional helicity (FDH) scheme [54] internally but automatically shifts the result

before output to the 't Hooft–Veltman scheme [55] using the full-color dependence in the shift. The approximation differs in these last two aspects from the one used in the earlier BlackHat calculation of W + 4-jet production [24]. This causes very slight shifts, under a percent, in our reported cross sections for W + n-jet production for $n \leq 4$ compared to ref. [24]. (A somewhat larger shift arises from the choice of a five-flavor scheme for the running of the coupling instead of the six-flavor scheme used earlier.)

The NLO result also requires real-emission corrections to the LO process, which arise from tree-level amplitudes with one additional parton; sample contributions are illustrated in fig. 2. For W production with four or five associated jets we use the COMIX code [41], included in the SHERPA framework [33], to compute these contributions, including the Catani-Seymour dipole subtraction terms [42]. The COMIX code is based on a color-dressed form [56] of the Berends-Giele recursion relations [57], making it very efficient for processes with high multiplicities. When there are fewer jets, we use the AMEGIC++ package [58] instead. In order to carry out the Monte Carlo integration over phase space we use an efficient hierarchical phase-space generator based on QCD antenna structures [59], as incorporated into SHERPA. The integration is performed using an adaptive alogorithm [60]. Running the algorithm in a stable and convergent manner for the real-emission contributions is highly nontrivial, in particular given the intricate structure of their infrared subtractions.

In general, the same physical distributions need to be analyzed at different PDF error sets, different renormalization or factorization scales, and for different jet algorithms or experimental cuts. We have organized the computation so the matrix elements do not have to be reevaluated for each choice of parameters [34]. For each event we generate, we record the momenta for all partons, along with the numerical values of the coefficients of the various scale- or PDF-dependent functions. Each term contains a simple function we wish to vary, such as a logarithm of the renormalization scale, multiplied by a numerical coefficient independent of such variation. We store the intermediate information in root-format n-tuple files [40]. At the end of the main computation we assemble the stored matrix-element coefficients, the PDF and scale choices to obtain cross sections. The availability of these intermediate results makes it straightforward to evaluate cross sections flexibly, for different scales, PDF error sets, experimental cuts or jet-based observables. This format has also been used by the experimental collaborations to compare results from BlackHat + SHERPA to experimental data [6].

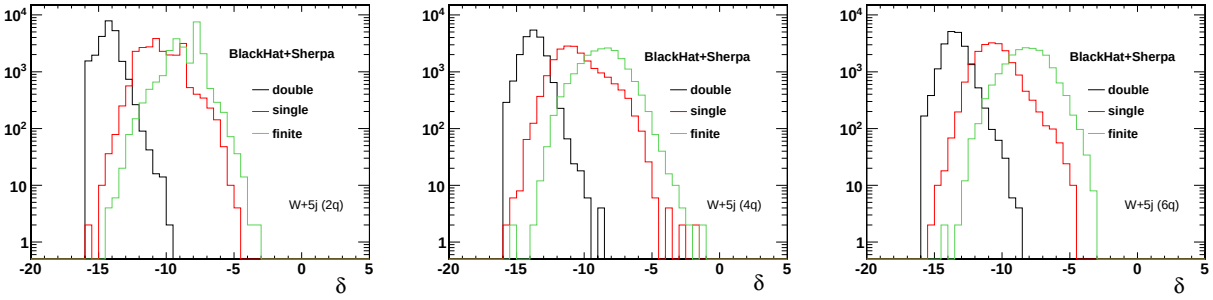

FIG. 3: The distribution of the relative error in the virtual cross section for three subprocesses, $gd \to e^- \bar{\nu}_e gggguu$, $ud \to e^- \bar{\nu}_e ggguu$ and $ud \to e^- \bar{\nu}_e guus\bar{s}$, reading from left to right. The horizontal axis is the logarithm of the relative error (2.6) between an evaluation by BlackHat, running in production mode, and a target expression evaluated at higher precision. The vertical axis shows the number of phase-space points having that relative error. The dark (black) line labeled by "double" shows the $1/\epsilon^2$ term; the darkly shaded (red) curve labeled by "single", the $1/\epsilon$ term; and the lightly shaded (green) curve labeled by "finite", the finite (ϵ^0) term. Each plot is based on approximately 10,000 points in phase space, distributed as in the actual calculation.

C. Numerical Stability

The different terms in the virtual contributions to matrix elements typically contain poles at unphysical locations in phase space. These poles cancel out when summing over all terms. When different terms are computed independently, one must ensure that the numerical precision of the computations suffices for cancellation of these spurious singularities anywhere in the phase space, so as to avoid unwanted loss of precision in the full matrix element. While the degree of the spurious singularities is in fact typically lower when using on-shell methods than with traditional ones, they are nonetheless present. They may cancel between coefficients of different integrals, each computed numerically. Obtaining a numerically stable result for the virtual terms at each point in phase space is accordingly nontrivial.

The BlackHat code detects instabilities following the criteria described in refs. [22, 32]. When faced with an unstable point in phase space, the code switches to higher precision arithmetic, and recomputes only those terms which suffer from the instability. The higher-precision computations are performed in software rather than in hardware, and are accordingly much slower than those at native precision. The recomputation of a limited number

of terms (as opposed to the entire amplitude) minimizes the additional computer time. We use the QD package [61] for higher-precision arithmetic.

In fig. 3, we illustrate the stability of the virtual contribution to the differential cross section, $d\sigma_V$, summed over colors and over all helicity configurations for the three subprocesses, $gd \to e^-\bar{\nu}_e ggggu$ and $ud \to e^-\bar{\nu}_e ggguu$ and $ud \to e^-\bar{\nu}_e guus\bar{s}$. In each plot, the horizontal axis represents the logarithmic error,

$$\delta = \log_{10}\left(\frac{|d\sigma_V^{\rm BH} - d\sigma_V^{\rm target}|}{|d\sigma_V^{\rm target}|}\right), \tag{2.6}$$

for each of the three components: $1/\epsilon^2$, $1/\epsilon$ and ϵ^0, where $\epsilon = (4-D)/2$ is the dimensional regulator. In eq. (2.6), $d\sigma_V^{\rm BH}$ is the cross section computed by BlackHat as it normally operates. The target value $d\sigma_V^{\rm target}$ is the cross section computed by BlackHat using multiprecision arithmetic with approximately 32 digits, and approximately 64 digits if the point is deemed unstable using the criteria described in refs. [22, 32]. The phase-space points are selected in the same way as those used to compute cross sections. We note that an overwhelming majority of events are accurate to better than one part in 10^3 — that is, to the left of the '-3' mark on the horizontal axis. We have explicitly checked that the few points to the right of this mark produce completely negligible errors in the final cross section or distributions, as their cross-section values are not especially large.

III. RESULTS

We now present our NLO results for W + 5-jet production at the LHC. We first discuss the renormalization-scale dependence of the total cross section. Then we provide the total hadronic energy distribution as an example distribution. Finally we present results for the total cross sections for W^- + 5-jet and W^+ + 5-jet production and for the $p_{\rm T}$ distributions of the five jets.

A. Scale dependence

We expect perturbative results to be more stable under variation of the renormalization and factorization scales as the perturbative order is increased. The residual variability has been used as a proxy for the expected uncertainty due to higher-order corrections beyond

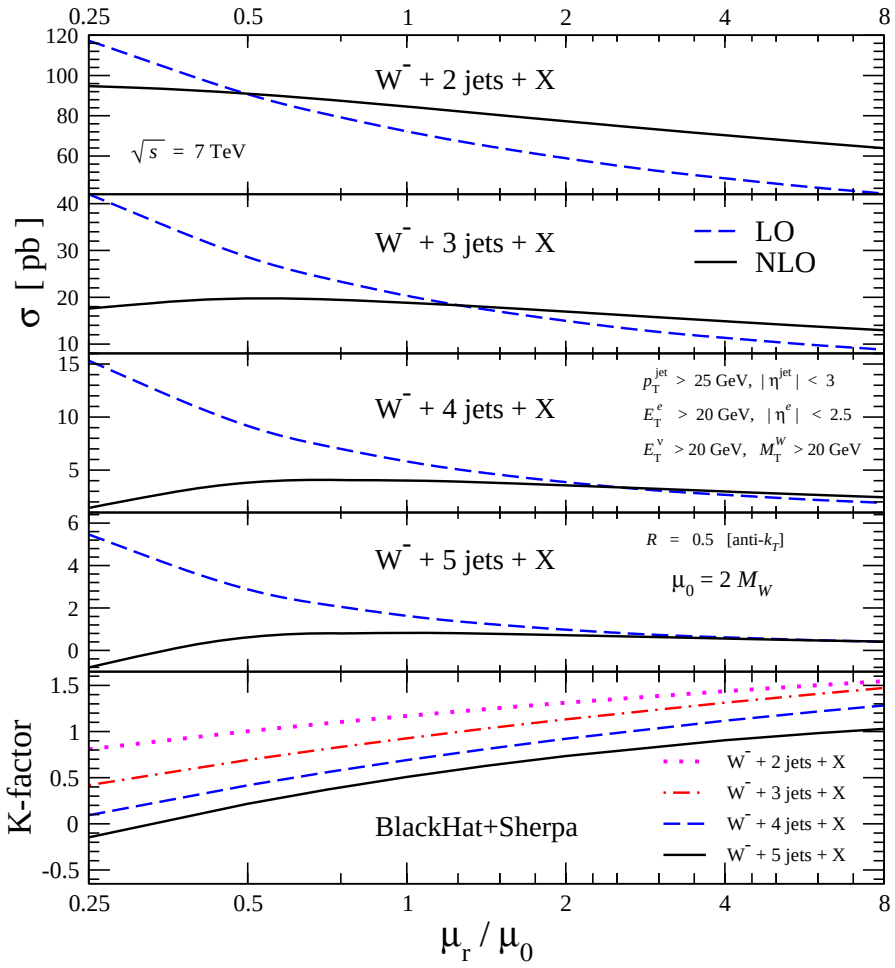

FIG. 4: The renormalization-scale dependence of the total cross section using a fixed reference scale of $\mu_0 = 2M_W$. The top four panels give the renormalization-scale dependence at both LO and NLO for W + 2-jets through W + 5-jets. The bottom panel shows the K factors for these cases, with the top curve for W + 2-jets and the bottom one for W + 5-jets. The factorization scale is held fixed.

the calculated order. In previous papers [22, 23], we have seen that the variability increases substantially with a growing number of jets at LO, but stabilizes at under 20% at NLO. This trend continues as the number of jets grows beyond the multiplicity considered in our just-cited studies. In fig. 4, we show the variation of the total cross section for W^- + n-jet production with the renormalization scale around a central choice of $\mu_0 = 2M_W$, for $n = 2, 3, 4, 5$ at LO and at NLO, along with the so-called "K factor," the ratio of the NLO to LO cross sections. We vary the scale down by a factor of four and upwards by a factor of eight. A fixed scale of $\mathcal{O}(M_W)$ is appropriate for the total cross section, as it is

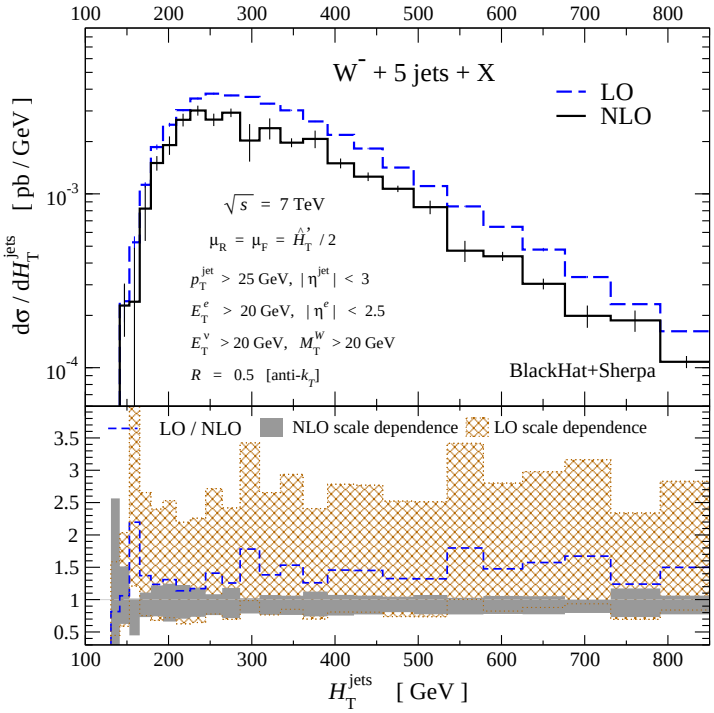

FIG. 5: The improvement in the renormalization and factorization scale dependence of the differential cross section as a function of the hadronic total transverse energy $H_{\mathrm{T}}^{\mathrm{jets}}$, comparing LO to NLO at the LHC at $\sqrt{s} = 7$ TeV. In the upper panels, the NLO predictions are shown as solid (black) lines, while the LO predictions are shown as dashed (blue) lines. The thin vertical line in the center of each bin (where visible) gives its numerical integration error, corresponding to the fluctuations in the plots. The lower panels show the predictions for the LO distribution and scale-dependence bands, normalized to the NLO prediction at the scale $\mu = \hat{H}'_{\mathrm{T}}/2$. The LO distribution is the dashed (blue) line, and the scale-dependence bands are shaded (gray) for NLO and cross-hatched (brown) for LO.

dominated by total transverse energies of the order of a small multiple of this scale. We hold the factorization scale fixed in order to eliminate changes in the PDFs as we vary the scale. This makes it simpler to see the trends as we change from two to five jets. Similar improvements in scale dependence are also observed when we include the variation of the factorization scale.

The four upper panels of fig. 4 show that the scale variation at NLO is greatly reduced with respect to that at LO. Furthermore, the LO variation grows substantially with an increasing number of jets, while the NLO variation is fairly stable. This increase is expected,

because there is an additional power of α_s for every additional jet; the variation of α_s is uncompensated at LO, but compensated at NLO by the virtual corrections. The relative stability of the NLO prediction in contrast to the LO one is also reflected in the bottom panel. As one increases the number of jets from the smallest (two), the K-factor curve steepens at first. This steepening slows down as the number of jets reaches five. This reflects a slowing down of the relative stabilization with growing number of jets. For the W + 5-jet process at LO, the change in the total cross section is on the order of a factor of 2 if we vary the renormalization scale by a factor of 2 around M_W as in fig. 4. In contrast, at NLO the dependence is cut to about $\pm 20\%$.

The distributions we study have a large dynamic range. Accordingly, for physics studies we choose an event-by-event scale to match typical energy scales individually rather than merely on average. Following ref. [22], we use a central scale equal to half the total partonic final-state transverse energy,

$$\mu_R = \mu_F = \mu = \hat{H}'_{\mathrm{T}}/2\,. \tag{3.1}$$

where $\hat{H}'_{\mathrm{T}}$ is defined in eq. (2.4). As an illustration of the scale dependence in a distribution using this choice, we show the variation of the LO and NLO W + 5-jet cross section as a function of the total jet transverse energy $H_{\mathrm{T}}^{\mathrm{jets}}$ in fig. 5. The bands in the figure show the results from varying the scale up and down by a factor of 2 around the central value (3.1), taking the minimum and maximum of the observable evaluated at five values: $\mu/2, \mu/\sqrt{2}, \mu, \sqrt{2}\mu, 2\mu$. The figure shows the markedly reduced scale dependence at NLO compared to that at LO. It also shows a remarkably flat ratio between the LO and NLO distributions. Other authors have suggested alternate choices of dynamical scale [27, 62].

B. Cross Sections and Distributions

In Table I, we present the LO and NLO parton-level cross sections for inclusive W^-- and W^+-boson production accompanied by one through five jets. As discussed in section II, we include all subprocesses (except for the IR-subtracted real-emission contributions with four quark pairs, which give contributions well under 1% using SHERPA's $\alpha_{\mathrm{dipole}} = 0.03$), and do a full-color sum everywhere except in the virtual contributions to $W + 4, 5$-jet production. In these latter contributions, we employ the leading-color approximation discussed in section II B, which has been validated to be accurate to better than 3% for W-boson

Jets	W^- LO	W^- NLO	W^+ LO	W^+ NLO
1	$284.0(0.1)^{+26.2}_{-24.6}$	$351.2(0.9)^{+16.8}_{-14.0}$	$416.8(0.6)^{+38.0}_{-35.5}$	$516(3)^{+29.}_{-23}$
2	$83.76(0.09)^{+25.45}_{-18.20}$	$83.5(0.3)^{+1.6}_{-5.2}$	$130.0(0.1)^{+39.3}_{-28.1}$	$125.1(0.8)^{+1.8}_{-7.4}$
3	$21.03(0.03)^{+10.66}_{-6.55}$	$18.3(0.1)^{+0.3}_{-1.8}$	$34.72(0.05)^{+17.44}_{-10.75}$	$29.5(0.2)^{+0.4}_{-2.8}$
4	$4.93(0.02)^{+3.49}_{-1.90}$	$3.87(0.06)^{+0.14}_{-0.62}$	$8.65(0.01)^{+6.06}_{-3.31}$	$6.63(0.07)^{+0.21}_{-1.03}$
5	$1.076(0.003)^{+0.985}_{-0.480}$	$0.77(0.02)^{+0.07}_{-0.19}$	$2.005(0.006)^{+1.815}_{-0.888}$	$1.45(0.04)^{+0.12}_{-0.34}$

TABLE I: Total cross sections in pb for $W + n$ jet production at the LHC at $\sqrt{s} = 7$ TeV, using the anti-k_T jet algorithm with $R = 0.5$. The NLO results for $W + 4, 5$-jet production use the leading-color approximation discussed in the text. The numerical integration uncertainty is given in parentheses, and the scale dependence is quoted in superscripts and subscripts.

production in association with up to four jets [22, 43].

In figs. 6 and 7, we show the $p_{\rm T}$ distributions for the five leading jets in W^- + 5-jet and W^+ + 5-jet production at $\sqrt{s} = 7$ TeV at the LHC. In the upper panels, we show the distributions at LO and NLO on a logarithmic scale. On this scale, the differences between distributions are not easily seen, so we display the ratios to the NLO prediction (with the central scale choice $\mu = \hat{H}'_{\rm T}/2$) in the lower panels. We also show the scale-dependence bands for both the LO and NLO predictions, again generated by varying the scale up and down by a factor of 2. We can see that the scale dependence is dramatically smaller at NLO, fulfilling one of the goals of the calculation. It makes the prediction of this high-multiplicity process truly quantitative. At larger transverse momenta for the leading two jets, the bands do show noticeable fluctuations because of limited statistics.

The overall normalization is not the only feature that changes in going from LO to NLO. The shape of the last-jet distribution appears to be the same at NLO (up to fluctuations from limited integration statistics), but all harder jets — four, in the present study — appear to have slightly softer distributions at NLO compared to LO. This continues a pattern seen previously in W + 3-jet [20, 22] and W + 4-jet [24] production.

In Table II, we present the charge-asymmetry ratio, which is the ratio between the production of a W^+ boson to a W^- boson, each accompanied by up to five jets. This ratio can be a sensitive probe of new physics [63]. The table also shows the jet-production ratios [7, 64] for either sign of the W charge, here defined by the ratio of the total cross section

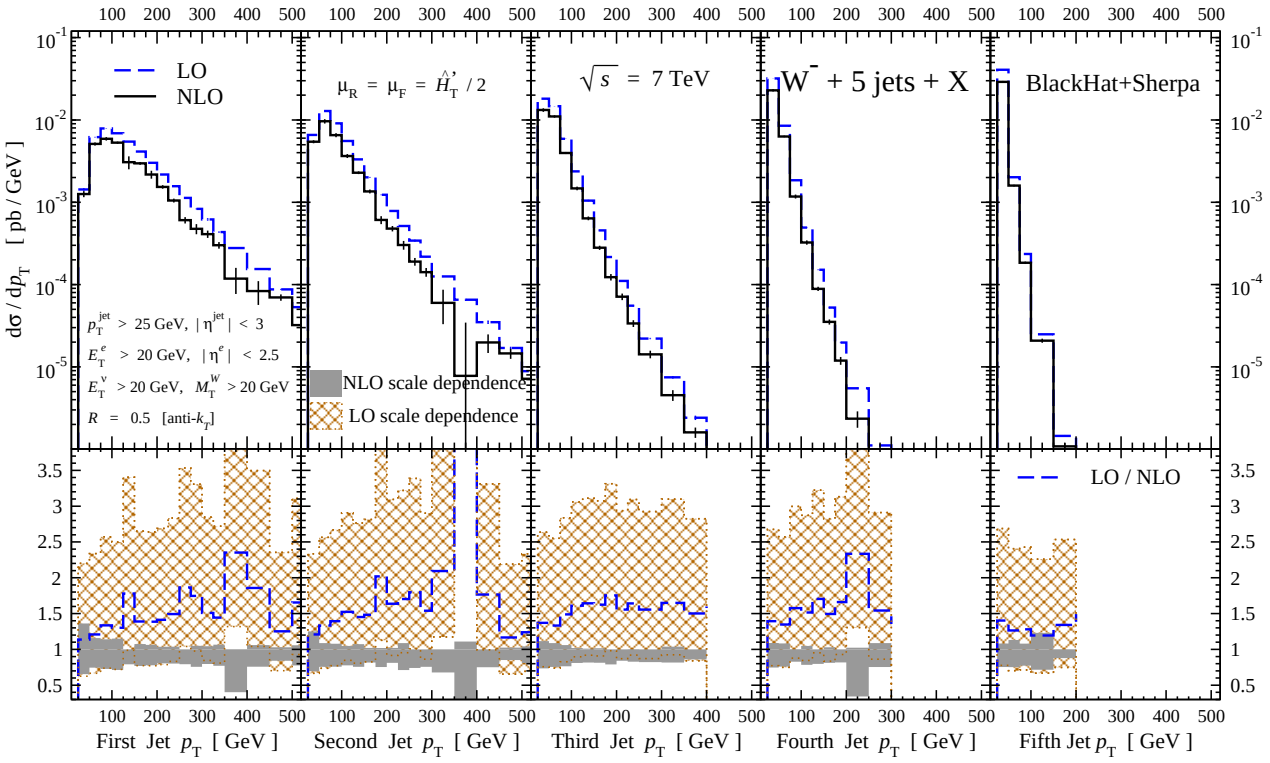

FIG. 6: The p_T distributions of the leading five jets in W^- + 5-jet production at the LHC at $\sqrt{s} = 7$ TeV. In the upper panels, the NLO predictions are shown as solid (black) lines, while the LO predictions are shown as dashed (blue) lines. The lower panels show the predictions for the LO distribution and scale-dependence bands normalized to the NLO prediction (at the scale $\mu = \hat{H}'_T/2$). The LO distribution is the dashed (blue) line, and the scale-dependence bands are shaded (gray) for NLO and cross-hatched (brown) for LO.

for $W^\pm$ + n-jet to $W^\pm$ + $(n-1)$-jet production. The charge-asymmetry ratios are all significantly greater than unity, and grow with increasing numbers of jets. The jet-production ratios are of order 1/4, and decrease with increasing numbers of jets. The NLO corrections to the charge-asymmetry are quite small, and the corrections to the jet-production ratios are modest but noticeable.

These values of the charge-asymmetry ratio reflect the excess of up quarks over down quarks in the proton. The W^+ bosons are necessarily emitted by up-type quarks, whereas $^-$ bosons are emitted by down-type quarks. The up-quark excess in the proton then leads to larger W^+ cross sections. As the number of jets increases, production of a W requires a larger value of the momentum fraction x. This alters the mix of subprocesses that contribute

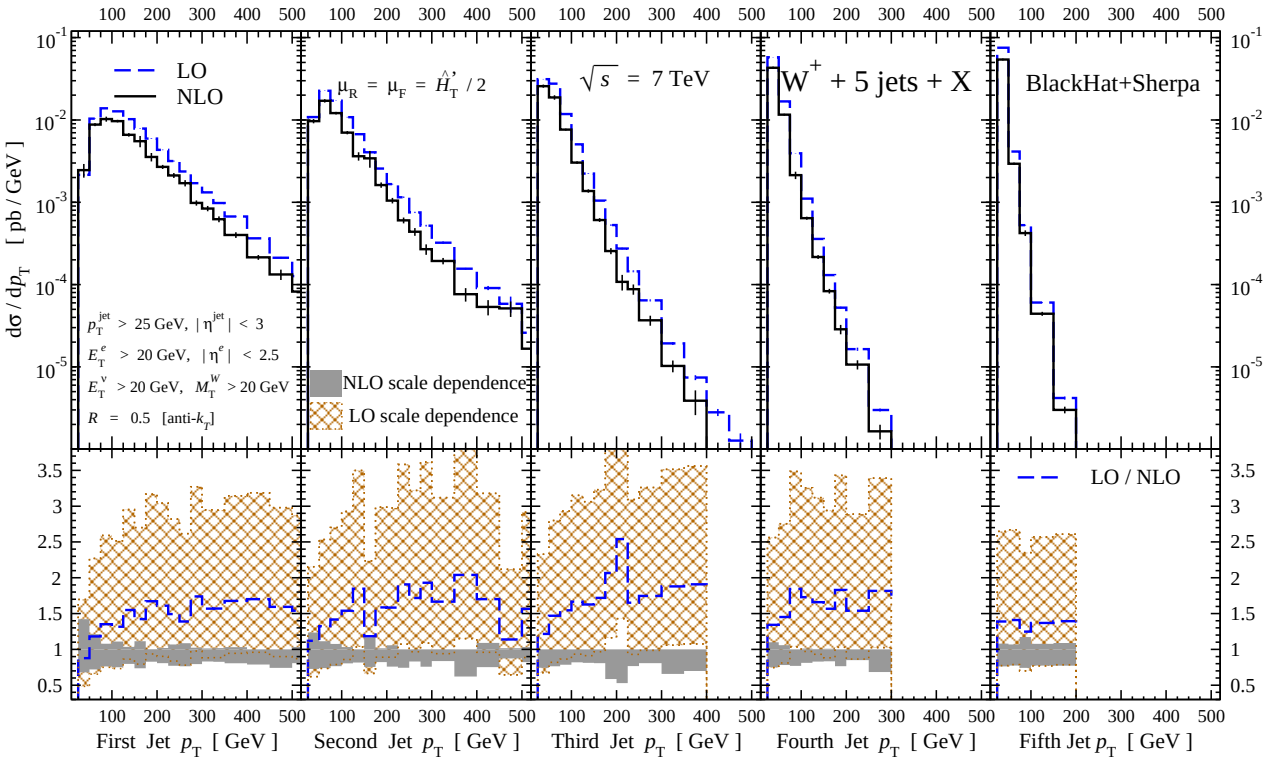

FIG. 7: The p_T distributions of the leading five jets in $W^+ +$ 5-jet production at the LHC at $\sqrt{s} = 7$ TeV.

Jets	W^+/W^-		$\frac{W^- + n}{W^- + (n-1)}$		$\frac{W^+ + n}{W^+ + (n-1)}$	
	LO	NLO	LO	NLO	LO	NLO
1	1.467(0.002)	1.47(0.01)	—	—	—	—
2	1.552(0.002)	1.50(0.01)	0.2949(0.0003)	0.238(0.001)	0.3119(0.0005)	0.242(0.002)
3	1.651(0.003)	1.61(0.01)	0.2511(0.0005)	0.220(0.001)	0.2671(0.0004)	0.235(0.002)
4	1.753(0.006)	1.72(0.03)	0.2345(0.0008)	0.211(0.003)	0.2490(0.0005)	0.225(0.003)
5	1.864(0.008)	1.87(0.06)	0.218(0.001)	0.200(0.006)	0.2319(0.0008)	0.218(0.006)

TABLE II: The first two columns give cross-section ratios for W^+ production to W^- production, as a function of the number of associated jest. The last two columns give the ratios of the cross section for the given process to that with one fewer jet. The numerical integration uncertainty is in parentheses.

to vector-boson production, and also increases the $u(x)/d(x)$ ratio. The case of $W +$ 1-jet production is special, because the gg initial state is absent at LO. In general, the gg initial

state contribution is expected to decrease with increasing x; but for W production this contribution actually increases with the number of jets, for production in association with two through four jets (judged by LO fractions); only for more than four jets does it start to decrease as expected. (In W^+ production, it starts to decrease above three rather than four accompanying jets.) The qg initial state decreases, but the qq initial state increases; the net effect, along with the increase in the $u(x)/d(x)$ fraction, is an increase in the W^+/W^- ratio. The results presented here extend our previous NLO analysis of these ratios with up to four accompanying jets [24] to the case of five accompanying jets. Both the LO and the NLO ratios are quite insensitive to correlated variations of the renormalization and factorization scales in numerator and denominator, so we do not quote the variation here, and only show the uncertainty from the numerical integration.

The increase in typical values of x with increasing numbers of jets also reduces the values of both the strong coupling α_s and the derivatives of the parton distributions, leading to a decrease in the jet-production ratios. The double ratios — the ratios of the LO cross sections in the fifth column of table II to those in the third column, and of the NLO cross sections in the last column to those in the fourth column — are roughly constant, suggesting that the decrease is primarily due to the decrease of α_s with increasing scale.

We can use the ratios to extrapolate to larger number of jets for the cuts used in this study. (Substantially different cuts could give rise to different behavior.) While ratios involving W + 1-jet production behave differently from the rest, both because of strong kinematic constraints and because of missing production channels (at LO), the remaining ratios turn out to allow an excellent fit to a straight line. For the charge ratio ($W^+ + n$ to $W^- + n$), the results through W + 4-jet production would suffice to yield a non-trivial prediction; the ratio for W + 5-jet production confirms this prediction. For the jet-production ratios ($W^\pm + n$ to $W^\pm + (n-1)$), the W + 5- to W + 4-jet production ratio is essential to making a non-trivial prediction, as it provides a third point in the fit. While these extrapolations should not be taken to too large a number of jets n, we expect them to provide a reasonable prediction for n somewhat beyond five.

For the LO charge ratio with n jets, we obtain the following prediction ($n \geq 2$),

$$R^{\rm LO}_{W^+/W^-} = 1.347 \pm 0.006 + (0.102 \pm 0.002)\, n\,; \tag{3.2}$$

for the NLO ratio,

$$R^{\rm NLO}_{W^+/W^-} = 1.27 \pm 0.03 + (0.11 \pm 0.01)\, n\,. \tag{3.3}$$

For the W^- jet-production ratio at LO, we find the following prediction ($n \geq 3$),

$$R^{{\rm LO},\,W^-}_{n/(n-1)} = 0.301 \pm 0.002 - (0.0165 \pm 0.0005)\, n\,; \tag{3.4}$$

at NLO, we find,

$$R^{{\rm NLO},\,W^-}_{n/(n-1)} = 0.248 \pm 0.008 - (0.009 \pm 0.002)\, n\,. \tag{3.5}$$

Similarly, for the W^+ jet-production ratio at LO, we find the following prediction ($n \geq 3$),

$$R^{{\rm LO},\,W^+}_{n/(n-1)} = 0.320 \pm 0.002 - (0.0177 \pm 0.0004)\, n\,; \tag{3.6}$$

and at NLO, we find,

$$R^{{\rm NLO},\,W^+}_{n/(n-1)} = 0.263 \pm 0.009 - (0.009 \pm 0.003)\, n\,. \tag{3.7}$$

The slopes for W^+ and W^- differ slightly at LO but are essentially the same at NLO. These predictions are based on fits to the data in table II. (More precisely, they are based on an ensemble of 10,000 fits to synthetic data distributed in a Gaussian according to the cross sections and statistical error in table I from which the ratios in table II were computed.)

From eqs. (3.5) and (3.7), we obtain the following predictions for the NLO cross sections for production of a $W^\pm$ in association with six jets,

$$\begin{aligned} W^- + 6 \text{ jets}: &\quad 0.15 \pm 0.01 \text{ pb}\,, \\ W^+ + 6 \text{ jets}: &\quad 0.30 \pm 0.03 \text{ pb}\,, \end{aligned} \tag{3.8}$$

matching the experimental cuts used for table I. The ratio of these two predictions, 2.0 ± 0.3, is consistent with an extrapolation using eq. (3.3), 1.94 ± 0.08.

IV. CONCLUSIONS

In this paper, we presented the first NLO QCD results for inclusive W + 5-jet production at the LHC at $\sqrt{s} = 7$ TeV. This process is an important background to many new physics searches involving missing energy, as well as to precise top-quark measurements. In addition to its phenomenological usefulness, it also sets a new bar for the state of the art in

perturbative QCD at next-to-leading order, at hadron-collider processes with six final-state objects including jets.

We have adopted a number of approximations in this work: the leading-color approximation for the virtual terms; neglecting top-quark loops; and neglecting infrared-finite parts of real-emission contributions with four quark pairs. Based on studies of W + 4-jet production and W production in associated with fewer jets [22, 43], we expect the leading-color approximation to change cross sections by no more than 3%, and the other approximations to be smaller yet. Hence these approximations should have no phenomenological significance, given the other theoretical uncertainties.

We find a dramatic reduction in scale dependence in NLO predictions for the total cross section, and for differential distributions as well. The scale dependence of observables shrinks from more than a factor of two variation at LO to a 20% sensitivity at NLO for W + 5-jet production. With our dynamical scale choice in eq. (2.4), we find K factors typically between 1 and 1.5, with moderate though non-trivial changes in shapes of distributions.

We have studied a number of ratios, between W^+ and W^- production, and for processes differing by the addition of one jet. The QCD corrections to these ratios are more modest than to total cross sections, and they should also benefit from milder experimental systematical uncertainties. The ratios show interesting trends with increasing number of jets, and with results for W + 5-jet production in hand, we can make plausible extrapolations to results for additional jets. These ratios also probe the evolution of different subprocesses with increasing parton fraction x.

The present study brings an unprecedented level of precision to W + 5-jet production. We look forward to comparing the NLO results for this process, and for the extrapolations to yet higher numbers of jets based upon it, with LHC data.

We thank Joey Huston, David Saltzberg, Maria Spiropulu, Gerben Stavenga, Eric Takasugi and Matthias Webber for helpful discussions. This research was supported by the US Department of Energy under contracts DE–FG03–91ER40662 and DE–AC02–76SF00515. DAK's research is supported by the European Research Council under Advanced Investigator Grant ERC–AdG–228301. DM's work was supported by the Research Executive Agency (REA) of the European Union under the Grant Agreement number PITN–GA–2010–264564 (LHCPhenoNet). The work of KJO and SH was partly supported by a grant from the US LHC Theory Initiative through NSF contract PHY–0705682. This research used resources

of Academic Technology Services at UCLA, and of the National Energy Research Scientific Computing Center, which is supported by the Office of Science of the U.S. Department of Energy under Contract No. DE–AC02–05CH11231.

---

[1] G. Aad *et al.* [ATLAS Collaboration], Phys. Lett. B **716**, 1 (2012) [arXiv:1207.7214 [hep-ex]].

[2] S. Chatrchyan *et al.* [CMS Collaboration], Phys. Lett. B **716**, 30 (2012) [arXiv:1207.7235 [hep-ex]].

[3] F. Abe *et al.* [CDF Collaboration], Phys. Rev. Lett. **70**, 4042 (1993); Phys. Rev. Lett. **79**, 4760 (1997) [hep-ex/9709016];
T. Aaltonen *et al.* [CDF Collaboration], Phys. Rev. D **77**, 011108 (2008) [arXiv:0711.4044 [hep-ex]].

[4] V. M. Abazov *et al.* [D0 Collaboration], Phys. Lett. B **705**, 200 (2011) [arXiv:1106.1457 [hep-ex]]; arXiv:1302.6508 [hep-ex].

[5] G. Aad *et al.* [ATLAS Collaboration], Phys. Lett. B **698**, 325 (2011) [arXiv:1012.5382 [hep-ex]]; arXiv:1301.6872 [hep-ex].

[6] G. Aad *et al.* [ATLAS Collaboration], Phys. Rev. D **85**, 032009 (2012) [arXiv:1111.2690 [hep-ex]];
G. Aad *et al.* [ATLAS Collaboration], Phys. Rev. D **85**, 092002 (2012) [arXiv:1201.1276 [hep-ex]].

[7] S. Chatrchyan *et al.* [CMS Collaboration], JHEP **1201**, 010 (2012) [arXiv:1110.3226 [hep-ex]]; Phys. Rev. Lett. **109**, 251801 (2012) [arXiv:1208.3477 [hep-ex]].

[8] P. B. Arnold and M. H. Reno, Nucl. Phys. B **319**, 37 (1989) [Erratum-ibid. B **330**, 284 (1990)]; P. B. Arnold, R. K. Ellis and M. H. Reno, Phys. Rev. D **40**, 912 (1989).

[9] J. M. Campbell and R. K. Ellis, Phys. Rev. D **65**, 113007 (2002) [hep-ph/0202176].

[10] F. Febres Cordero, L. Reina and D. Wackeroth, Phys. Rev. D **74**, 034007 (2006) [hep-ph/0606102];
J. M. Campbell, R. K. Ellis, F. Febres Cordero, F. Maltoni, L. Reina, D. Wackeroth and S. Willenbrock, Phys. Rev. D **79**, 034023 (2009) [arXiv:0809.3003 [hep-ph]].

[11] Z. Bern, L. J. Dixon, D. C. Dunbar and D. A. Kosower, Nucl. Phys. B **425**, 217 (1994) [hep-ph/9403226]; Nucl. Phys. B **435**, 59 (1995) [hep-ph/9409265].

[12] Z. Bern and A. G. Morgan, Nucl. Phys. B **467**, 479 (1996) [hep-ph/9511336];
Z. Bern, L. J. Dixon, D. C. Dunbar and D. A. Kosower, Phys. Lett. B **394** (1997) 105 [hep-th/9611127];
C. Anastasiou, R. Britto, B. Feng, Z. Kunszt and P. Mastrolia, Phys. Lett. B **645** (2007) 213 [hep-ph/0609191];
R. Britto and B. Feng, JHEP **0802**, 095 (2008) [arXiv:0711.4284 [hep-ph]];
W. T. Giele, Z. Kunszt and K. Melnikov, JHEP **0804**, 049 (2008) [arXiv:0801.2237 [hep-ph]];
R. Britto, B. Feng and P. Mastrolia, Phys. Rev. D **78**, 025031 (2008) [arXiv:0803.1989 [hep-ph]];
R. K. Ellis, W. T. Giele, Z. Kunszt and K. Melnikov, Nucl. Phys. B **822** (2009) 270 [arXiv:0806.3467 [hep-ph]].

[13] Z. Bern, L. J. Dixon and D. A. Kosower, Nucl. Phys. B **513**, 3 (1998) [hep-ph/9708239].

[14] R. Britto, F. Cachazo and B. Feng, Nucl. Phys. B **725**, 275 (2005) [hep-th/0412103].

[15] R. Britto, F. Cachazo, B. Feng and E. Witten, Phys. Rev. Lett. **94**, 181602 (2005) [hep-th/0501052].

[16] C. F. Berger, Z. Bern, L. J. Dixon, D. Forde and D. A. Kosower, Phys. Rev. D **74**, 036009 (2006) [hep-ph/0604195].

[17] G. Ossola, C. G. Papadopoulos and R. Pittau, Nucl. Phys. B **763**, 147 (2007) [hep-ph/0609007].

[18] D. Forde, Phys. Rev. D **75**, 125019 (2007) [arXiv:0704.1835 [hep-ph]].

[19] S. D. Badger, JHEP **0901**, 049 (2009) [arXiv:0806.4600 [hep-ph]].

[20] C. F. Berger, Z. Bern, L. J. Dixon, F. Febres Cordero, D. Forde, T. Gleisberg, H. Ita, D. A. Kosower and D. Maître, Phys. Rev. Lett. **102**, 222001 (2009) [arXiv:0902.2760 [hep-ph]].

[21] R. K. Ellis, K. Melnikov and G. Zanderighi, JHEP **0904**, 077 (2009) [arXiv:0901.4101 [hep-ph]]; Phys. Rev. D **80**, 094002 (2009) [arXiv:0906.1445 [hep-ph]].

[22] C. F. Berger, Z. Bern, L. J. Dixon, F. Febres Cordero, D. Forde, T. Gleisberg, H. Ita, D. A. Kosower and D. Maître, Phys. Rev. D **80**, 074036 (2009) [arXiv:0907.1984 [hep-ph]].

[23] C. F. Berger, Z. Bern, L. J. Dixon, F. Febres Cordero, D. Forde, T. Gleisberg, H. Ita, D. A. Kosower and D. Maître, Phys. Rev. D **82**, 074002 (2010) [arXiv:1004.1659 [hep-ph]].

[24] C. F. Berger, Z. Bern, L. J. Dixon, F. Febres Cordero, D. Forde, T. Gleisberg, H. Ita, D. A. Kosower and D. Maître, Phys. Rev. Lett. **106**, 092001 (2011) [arXiv:1009.2338 [hep-ph]].

[25] H. Ita, Z. Bern, L. J. Dixon, F. Febres Cordero, D. A. Kosower and D. Maître, Phys. Rev. D **85**, 031501 (2012) [arXiv:1108.2229 [hep-ph]].

[26] T. Melia, K. Melnikov, R. Röntsch and G. Zanderighi, JHEP **1012**, 053 (2010) [arXiv:1007.5313 [hep-ph]]; Phys. Rev. D **83**, 114043 (2011)[arXiv:1104.2327 [hep-ph]].

[27] A. Bredenstein, A. Denner, S. Dittmaier and S. Pozzorini, JHEP **1003**, 021 (2010) [arXiv:1001.4006 [hep-ph]].

[28] G. Bevilacqua, M. Czakon, C. G. Papadopoulos, R. Pittau and M. Worek, JHEP **0909**, 109 (2009) [arXiv:0907.4723 [hep-ph]];
G. Bevilacqua, M. Czakon, C. G. Papadopoulos and M. Worek, Phys. Rev. Lett. **104**, 162002 (2010) [arXiv:1002.4009 [hep-ph]]; Phys. Rev. D **84**, 114017 (2011) [arXiv:1108.2851 [hep-ph]].

[29] S. Becker, D. Goetz, C. Reuschle, C. Schwan and S. Weinzierl, Phys. Rev. Lett. **108**, 032005 (2012) [arXiv:1111.1733 [hep-ph]].

[30] A. Bredenstein, A. Denner, S. Dittmaier and S. Pozzorini, JHEP **0808**, 108 (2008) [arXiv:0807.1248 [hep-ph]]; Phys. Rev. Lett. **103**, 012002 (2009) [arXiv:0905.0110 [hep-ph]];
T. Binoth, N. Greiner, A. Guffanti, J. P. Guillet, T. Reiter and J. Reuter, Phys. Lett. B **685**, 293 (2010) [arXiv:0910.4379 [hep-ph]].

[31] F. Cascioli, P. Maierhofer and S. Pozzorini, Phys. Rev. Lett. **108**, 111601 (2012) [arXiv:1111.5206 [hep-ph]].

[32] C. F. Berger, Z. Bern, L. J. Dixon, F. Febres Cordero, D. Forde, H. Ita, D. A. Kosower and D. Maître, Phys. Rev. D **78**, 036003 (2008) [arXiv:0803.4180 [hep-ph]].

[33] T. Gleisberg, S. Höche, F. Krauss, A. Schälicke, S. Schumann and J. C. Winter, JHEP **0402**, 056 (2004) [hep-ph/0311263];
T. Gleisberg, S. Höche, F. Krauss, M. Schönherr, S. Schumann, F. Siegert and J. Winter, JHEP **0902**, 007 (2009) [arXiv:0811.4622 [hep-ph]].

[34] Z. Bern, G. Diana, L. J. Dixon, F. Febres Cordero, S. Höche, D. A. Kosower, H. Ita, D. Maître and K. Ozeren, Phys. Rev. Lett. **109**, 042001 (2012) [arXiv:1112.3940 [hep-ph]].

[35] Z. Bern, G. Diana, L. J. Dixon, F. Febres Cordero, D. Forde, T. Gleisberg, S. Höche, H. Ita, D. A. Kosower, D. Maître and K. Ozeren, Phys. Rev. D **84**, 034008 (2011) [arXiv:1103.5445 [hep-ph]].

[36] Z. Bern, G. Diana, L. J. Dixon, F. Febres Cordero, S. Höche, H. Ita, D. A. Kosower, D. Maître and K. J. Ozeren, Phys. Rev. D **84**, 114002 (2011) [arXiv:1106.1423 [hep-ph]].

[37] Z. Bern, G. Diana, L. J. Dixon, F. Febres Cordero, S. Höche, H. Ita, D. A. Kosower, D. Maître and K. J. Ozeren, Phys. Rev. D **87**, 034026 (2013) [arXiv:1206.6064 [hep-ph]].

[38] S. Chatrchyan *et al.* [CMS Collaboration], JHEP **1108**, 155 (2011) [arXiv:1106.4503 [hep-ex]]; S. Chatrchyan *et al.* [CMS Collaboration], Phys. Rev. Lett. **109**, 171803 (2012) [arXiv:1207.1898 [hep-ex]].

[39] G. Ossola, C. G. Papadopoulos and R. Pittau, JHEP **0803**, 042 (2008) [arXiv:0711.3596 [hep-ph]];
J.-C. Winter and W. T. Giele, arXiv:0902.0094 [hep-ph];
P. Mastrolia, G. Ossola, T. Reiter and F. Tramontano, JHEP **1008**, 080 (2010) [arXiv:1006.0710 [hep-ph]];
G. Bevilacqua, M. Czakon, M. V. Garzelli, A. van Hameren, A. Kardos, C. G. Papadopoulos, R. Pittau and M. Worek, Comput. Phys. Commun. **184**, 986 (2013) [arXiv:1110.1499 [hep-ph]];
G. Cullen, N. Greiner, G. Heinrich, G. Luisoni, P. Mastrolia, G. Ossola, T. Reiter and F. Tramontano, Eur. Phys. J. C **72**, 1889 (2012) [arXiv:1111.2034 [hep-ph]];
S. Badger, B. Biedermann, P. Uwer and V. Yundin, Phys. Lett. B **718**, 965 (2013) [arXiv:1209.0098 [hep-ph]]; arXiv:1209.0100 [hep-ph].

[40] R. Brun and F. Rademakers, Nucl. Instrum. Meth. A **389**, 81 (1997).

[41] T. Gleisberg and S. Höche, JHEP **0812**, 039 (2008) [arXiv:0808.3674 [hep-ph]].

[42] S. Catani and M. H. Seymour, Nucl. Phys. B **485**, 291 (1997) [Erratum-ibid. B **510**, 503 (1998)] [hep-ph/9605323].

[43] H. Ita and K. Ozeren, JHEP **1202**, 118 (2012) [arXiv:1111.4193 [hep-ph]].

[44] M. Cacciari, G. P. Salam and G. Soyez, JHEP **0804**, 063 (2008) [arXiv:0802.1189 [hep-ph]].

[45] S. Catani, Y. L. Dokshitzer, M. H. Seymour and B. R. Webber, Nucl. Phys. B **406**, 187 (1993); G. P. Salam and G. Soyez, JHEP **0705**, 086 (2007) [arXiv:0704.0292 [hep-ph]].

[46] M. Cacciari, G. P. Salam and G. Soyez, Eur. Phys. J. C **72**, 1896 (2012) [arXiv:1111.6097 [hep-ph]].

[47] A. D. Martin, W. J. Stirling, R. S. Thorne and G. Watt, Eur. Phys. J. C **63**, 189 (2009) [arXiv:0901.0002 [hep-ph]].

[48] S. Frixione and B. R. Webber, JHEP **0206**, 029 (2002) [hep-ph/0204244];
P. Nason, JHEP **0411**, 040 (2004) [hep-ph/0409146];

S. Frixione, P. Nason and C. Oleari, JHEP **0711**, 070 (2007) [0709.2092 [hep-ph]].

[49] S. Alioli, P. Nason, C. Oleari and E. Re, JHEP **1006**, 043 (2010) [1002.2581 [hep-ph]];
K. Hamilton and P. Nason, JHEP **1006**, 039 (2010) [1004.1764 [hep-ph]];
S. Höche, F. Krauss, M. Schönherr and F. Siegert, JHEP **1104**, 024 (2011) [arXiv:1008.5399 [hep-ph]]; JHEP **1108**, 123 (2011) [arXiv:1009.1127 [hep-ph]];
R. Frederix, S. Frixione, V. Hirschi, F. Maltoni, R. Pittau and P. Torrielli, Phys. Lett. B **701**, 427 (2011) [arXiv:1104.5613 [hep-ph]]; JHEP **1109**, 061 (2011) [arXiv:1106.6019 [hep-ph]].

[50] N. Lavesson and L. Lönnblad, JHEP **0812**, 070 (2008) [arXiv:0811.2912 [hep-ph]];
S. Höche, F. Krauss, M. Schönherr and F. Siegert, arXiv:1207.5030 [hep-ph];
T. Gehrmann, S. Höche, F. Krauss, M. Schönherr and F. Siegert, JHEP **1301**, 144 (2013) [arXiv:1207.5031 [hep-ph]];
L. Lönnblad and S. Prestel, JHEP **1302**, 094 (2013) [arXiv:1211.4827 [hep-ph]]; arXiv:1211.7278 [hep-ph];
S. Alioli, C. W. Bauer, C. J. Berggren, A. Hornig, F. J. Tackmann, C. K. Vermilion, J. R. Walsh and S. Zuberi, arXiv:1211.7049 [hep-ph];
K. Hamilton, P. Nason, C. Oleari and G. Zanderighi, arXiv:1212.4504 [hep-ph].

[51] Z. Bern, L. J. Dixon and D. A. Kosower, Ann. Rev. Nucl. Part. Sci. **46** (1996) 109 [hep-ph/9602280];
Z. Bern, L. J. Dixon and D. A. Kosower, Annals Phys. **322** (2007) 1587 [arXiv:0704.2798 [hep-ph]];
R. Britto, J. Phys. A **44** (2011) 454006 [arXiv:1012.4493 [hep-th]];
H. Ita, J. Phys. A **44** (2011) 454005 [arXiv:1109.6527 [hep-th]];
R. K. Ellis, Z. Kunszt, K. Melnikov and G. Zanderighi, Phys. Rept. **518** (2012) 141 [arXiv:1105.4319 [hep-ph]].

[52] W. T. Giele and G. Zanderighi, JHEP **0806** (2008) 038 [arXiv:0805.2152 [hep-ph]].

[53] Z. Bern, L. J. Dixon and D. A. Kosower, Nucl. Phys. B **437**, 259 (1995) [hep-ph/9409393].

[54] Z. Bern and D. A. Kosower, Nucl. Phys. B **379**, 451 (1992);
Z. Bern, A. De Freitas, L. J. Dixon and H. L. Wong, Phys. Rev. D **66**, 085002 (2002) [hep-ph/0202271].

[55] G. 't Hooft and M. Veltman, Nucl. Phys. B **44**, 189 (1972).

[56] C. Duhr, S. Höche and F. Maltoni, JHEP **0608**, 062 (2006) [hep-ph/0607057].

[57] F. A. Berends and W. T. Giele, Nucl. Phys. B **306**, 759 (1988).

[58] F. Krauss, R. Kuhn and G. Soff, JHEP **0202**, 044 (2002) [hep-ph/0109036];
T. Gleisberg and F. Krauss, Eur. Phys. J. C **53**, 501 (2008) [arXiv:0709.2881 [hep-ph]].

[59] A. van Hameren and C. G. Papadopoulos, Eur. Phys. J. C **25**, 563 (2002) [hep-ph/0204055];
T. Gleisberg, S. Höche and F. Krauss, arXiv:0808.3672 [hep-ph].

[60] G. P. Lepage, J. Comput. Phys. **27**, 192 (1978);
T. Ohl, Comput. Phys. Commun. **120**, 13 (1999) [hep-ph/9806432].

[61] Y. Hida, X. S. Li and D. H. Bailey, http://crd.lbl.gov/~dhbailey/mpdist, report LBNL-46996.

[62] C. W. Bauer and B. O. Lange, arXiv:0905.4739 [hep-ph];
K. Melnikov and G. Zanderighi, Phys. Rev. D **81**, 074025 (2010) [arXiv:0910.3671 [hep-ph]].

[63] C.-H. Kom and W. J. Stirling, Eur. Phys. J. C **69**, 67 (2010) [arXiv:1004.3404 [hep-ph]]; Eur. Phys. J. C **71**, 1546 (2011) [arXiv:1010.2988 [hep-ph]].

[64] S. D. Ellis, R. Kleiss and W. J. Stirling, Phys. Lett. B **154**, 435 (1985);
F. A. Berends *et al.*, Phys. Lett. B **224**, 237 (1989);
F. A. Berends, H. Kuijf, B. Tausk and W. T. Giele, Nucl. Phys. B **357**, 32 (1991);
E. Abouzaid and H. J. Frisch, Phys. Rev. D **68**, 033014 (2003) [hep-ph/0303088].